Cement and Concrete Composites 106 (2020) 103472

Contents lists available at ScienceDirect

Cement and Concrete Composites

journal homepage: http://www.elsevier.com/locate/cemconcomp

Nanostructural evolution of alkali-activated mineral wools

J. Yliniemi [a,*], B. Walkley [b,c], J.L. Provis [b], P. Kinnunen [a], M. Illikainen [a]

[a] Fibre and Particle Engineering Research Unit, University of Oulu, P.O. Box 4300, 90014, Oulu, Finland
[b] Department of Materials Science and Engineering, The University of Sheffield, Sir Robert Hadfield Building, Mappin St, Sheffield, S1 3JD, United Kingdom
[c] Department of Chemical and Biological Engineering, The University of Sheffield, Sir Robert Hadfield Building, Mappin St, Sheffield, S1 3JD, United Kingdom

ARTICLE INFO

Keywords:
Alkali-activated material
Mineral wool
Waste valorisation
X-ray diffraction
Electron microscopy
Nuclear magnetic resonance

ABSTRACT

Mineral wools are the most widely used building insulation material worldwide. Annually, 2.5 million tonnes of mineral wool waste are generated in the EU alone, and this is a largely unutilised material that is landfilled or incinerated. However, mineral wool wastes are promising precursors for production of alkali-activated cementitious binders due to their favourable chemical and mineralogical composition and high surface area. Alkali-activation is therefore a valuable route for valorisation of large quantities of mineral wool waste. This study resolves the phase assemblage and nanostructure of reaction products formed upon alkali activation of stone wool and glass wool by sodium hydroxide and sodium silicate solutions with X-ray diffraction, electron microscopy and solid state nuclear magnetic resonance spectroscopy experiments probing ^{27}Al and ^{29}Si. The stone wool-based alkali-activated binder comprises an amorphous sodium- and aluminium-substituted calcium silicate hydrate (C-(N-)A-S-H) gel, an amorphous sodium aluminosilicate hydrate (N-A-S-H) gel and small amounts of the layered double hydroxide phase quintinite and zeolite F. The glass wool-based alkali-activated binder comprises an amorphous Ca- and Al-substituted sodium silicate (N-(C-)(A-)S–H) gel. Gel chemical composition and reaction kinetics of alkali-activated mineral wools are shown to be dependent on the activating solution chemistry, with reaction rate and extent promoted by inclusion of a source of soluble Si in the reaction mixture. This work provides the most advanced description of the chemistry and structure of alkali-activated mineral wools to date, yielding new insight that is essential in developing valorisation pathways for mineral wools by alkali activation and providing significant impetus for development of sustainable construction materials.

1. Introduction

As an alternative to traditional clinker-based cements, alkali-activated materials (AAMs) have the capacity to reduce global CO_2 emissions and to utilise fly ashes, slags, and other mineral wastes that would otherwise end up in landfill [1,2]. However, for AAMs to be environmentally and economically competitive when compared with Portland cement (PC), precursor materials must be locally sourced so as to not require transportation across long distances [3]. Production of AAMs from local mineral wastes has therefore gained significant academic and commercial interest in recent years.

Mineral wool waste is generated in construction and demolition (C&D) of buildings and from mineral wool manufacturing, and is largely unutilised. Mineral wool-based building insulation is one of the most effective ways to achieve energy and cost savings associated with heating and cooling buildings. Consequently, the total amount of mineral wool waste globally is growing rapidly amidst continued urbanisation and demand for sustainable buildings. Mineral wools are the largest single waste source in some landfills on a volumetric basis.

The nomenclature of mineral wools includes the terms man-made vitreous fibre, man-made mineral fibre, mineral fibre, and mineral cotton. From these, mineral fibre is a generic term for all non-metallic inorganic fibres, whereas the term mineral wool includes glass wool, stone wool and slag wool, each indicating their precursor. Currently, stone wool is the principal type produced, glass wool is second, being produced at about one-third of the volume of stone wool, and slag wool is no longer produced in significant volumes [4].

While there are some differences in the manufacturing processes of stone and glass wools, the basic principle involves melting quartz, basalt, dolomite, recycled glass and other mineral raw materials at high temperatures [5]. The molten mixture is spun into fibres via a high-speed spinning process. To bind the fibres together organic resins (typically phenol-formaldehyde-based) are added. The amount of organic resin used depends on the product type, but it typically varies

* Corresponding author. Fibre and Particle Engineering Research Unit, P.O. Box 4300, 90014, University of Oulu, Finland.
E-mail address: juho.yliniemi@oulu.fi (J. Yliniemi).

https://doi.org/10.1016/j.cemconcomp.2019.103472
Received 6 May 2019; Received in revised form 4 November 2019; Accepted 18 November 2019
Available online 21 November 2019

between 2 and 11 wt%. A small amount of mineral oil may also be added to prevent dusting [6]. If mineral wool mats, slabs or boards are produced, a cutting process splits mineral wool according to its trade width which creates mineral wool cutting waste. Finally, the mineral wool is temporarily compressed down to a tenth of its volume to reduce transport and storage expenses.

Interestingly, mineral wools have favourable chemical composition and mineralogy for alkali activation. They are completely X-ray amorphous with high Si content. The main components of typical stone wool are SiO_2 (~40–45 wt%), Al_2O_3 (~14–18 wt%), (CaÕ15–18 wt%), and (MgO ~9–12 wt%), representing quite a different composition from any other major AAM precursor. The main components of glass wool are SiO_2 (~60–65 wt%), Na_2O (~16 wt%), and CaO (~7 wt%), which is similar to everyday soda-lime glass [7]. Mineral wool fibres have widths of approximately 10 μm [8] and hence exhibit high specific surface areas which increases their reactivity.

The total volume of mineral wool waste produced in the EU27 countries alone was 2.3 million tonnes in 2010, increasing to an expected 2.5 million tonnes annually by 2020 [9]. Current practice is to landfill this waste, which causes high costs for the C&D industry as well as for mineral wool producers. Utilising mineral wool waste as a source material for AAM production avoids the landfilling costs and can provide an avenue for additional profits for C&D and mineral wool manufacturing companies.

To date there are only two publications investigating alkali activation of mineral wools [10,11]. This work has shown that stone wool reacted with a sodium aluminate solution to form an X-ray amorphous gel, a partially dehydrated basic hydrosodalite phase ($Na_8(AlSiO_4)_6(OH)_2{\cdot}4H_2O$) and a partially dehydrated quintinite phase ($(Mg_4Al_2)(OH)_{12}CO_3(H_2O)_3)_{0.5}$ (part of the hydrotalcite group of layered double hydroxides (LDH)). In contrast, when glass wool was reacted with a sodium aluminate solution a dehydrated sodalite phase ($Na_6(AlSiO_4)_6$) and an X-ray amorphous gel were identified, with the absence of the hydrotalcite-group LDH phase attributed to the far lower MgO content in glass wool. Alkali-activated stone and glass wool exhibited compressive strengths at 28 days of curing of 30 MPa and 49 MPa, respectively. These attributes make alkali-activated mineral wools attractive for civil engineering and earth construction applications.

These early results have been promising, but have not revealed detailed information about the phase assemblage and nanostructure of the binder gel. We therefore resolve these details in a series of alkali-activated mineral wools displaying varied chemical composition and mineralogy by application of advanced spectroscopic and microstructural characterisation techniques including X-ray diffraction, electron microscopy and solid state nuclear magnetic resonance spectroscopy. This work provides the most advanced description of the chemistry and structure of alkali-activated mineral wools to date, and reveals new insight that is crucial for controlling the mechanical properties, physical and chemical durability of these materials. This provides a new platform of knowledge to drive valorisation of mineral wool wastes and increased sustainability in the construction industry.

2. Experimental

2.1. Sample preparation

2.1.1. Precursors

In order to eliminate the possible reactions with organic resin during alkali activation, mineral wool samples free of organics were collected from commercial sources prior to the addition of organic resins or other additives. Strictly speaking, these organic-free materials are mineral fibres, however because of the complex and often inconsistent nomenclature used to describe these materials we have chosen to use the generic term 'mineral wool' throughout the remainder of this article for simplicity. The chemical composition of each mineral wool as determined by X-ray fluorescence (XRF) is presented in Table 1. In addition to the major oxides given in Table 1, glass wool contains typically ~2–4 wt % B_2O_3 [11] which is not quantifiable with the XRF technique used here. Only moisture was evaporated when the samples were heated to 525 °C, which confirmed that samples were free of organic additives.

Before alkali activation the mineral wools were ground with a Germatec ball mill in a 10 L milling chamber for 3 h. Steel balls (150 pcs.), 25–40 mm in diameter, were used. The average lengths and widths of the milled fibres shown in Table 1 were analysed using a large tube-flow fractionation method as described previously [8]. The milling process was effective as the original average lengths of the fibres are several hundreds of micrometers [8]. However, as the average aspect ratio of the milled fibres is around 3 there is still some fibrous nature remaining. It should be noted that the camera resolution of large tube-flow fractionation method is 6.4 μm [8], thus a portion of smallest milled mineral wool particles are not detected, which increases the measured average fibre length and width.

Stone wool and glass wool fall within very different regions of the (CaO + MgO)–Al_2O_3–SiO_2 ternary system as shown in Fig. 1. The closest reference point for stone wool compared to other common AAM precursors is ground granulated blast furnace slag (GGBFS). However, GGBFS has more calcium (~40 wt % c.f. 15.3 wt %) and usually less MgO when compared with stone wool, which promotes formation of Ca-rich structures such as calcium silicate hydrate (C–S–H), aluminium-substituted calcium silicate hydrate (C-A-S-H) (in the presence of sufficient Al content) and Na- and Al-substituted calcium silicate hydrate (C-(N-)A-S-H) (in the presence of sufficient Na content) [12]. Glass wool is within the compositional region of other soda-lime silicate glasses i.e. everyday waste glass.

2.1.2. Preparation of alkali activators

Reagent grade NaOH pellets [Honeywell] were dissolved in distilled water to give a 6.25 mol/L NaOH solution. Sodium silicate solution was prepared by mixing bulk sodium silicate solution ([PQ Chemicals], supplied at 29.4 wt% SiO_2, 14.7 wt% Na_2O and 55.9 wt% H_2O) with distilled water. The final activator solution (denoted $Na_2O{\cdot}2SiO_2$) contained 24.5 wt% SiO_2, 12.3 wt% Na_2O and 63.3 wt% H_2O, with SiO_2/Na_2O molar modulus (Ms) of 2.0.

2.1.3. Preparation of alkali-activated mineral wools

Milled mineral wool was added continuously into the alkali activator according to the amounts outlined in Table 2. Mixing was done with a high shear mixer (Heidolph, RZR 2020) at 800 rpm with 7 min mixing time. Sample pastes were sealed into cylindrical plastic containers, vibrated to remove entrained air bubbles, and cured at 40 °C for 1 day

Table 1
Major oxide compositions and other characteristics of the stone wool (SW) and glass wool (GW) used in this study. Average fibre length and width of the milled mineral wool were determined as described in Ref. [8].

	Stone wool (SW)	Glass wool (GW)
SiO_2 (wt.%)	39.9	63.3
Al_2O_3 (wt.%)	14.8	1.5
CaO (wt.%)	15.3	8.2
MgO (wt.%)	10.9	3.1
Fe_2O_3 (wt.%)	11.6	0.5
Na_2O (wt.%)	2.0	16.5
K_2O (wt.%)	0.8	0.5
P_2O_5 (wt.%)	0.3	0.2
SO_3 (wt.%)	0.1	0.2
TiO_2 (wt.%)	2.1	0.0
Others (wt.%) [a]	2.2	6.0
Moisture content (wt.%)	0.06	0.02
Loss-on-ignition 525 °C (wt.%)	0.0	0.06
Average fibre length [μm]	29	32
Average fibre width [μm]	10	10

[a] Glass wool typically contains 2–4 wt % B_2O_5, which is not detectable using X-ray fluorescence.

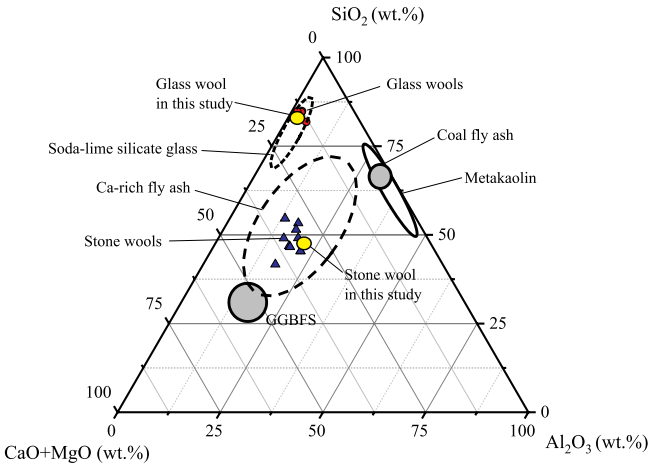

Fig. 1. Ternary diagram showing the chemical composition (mass basis) of stone wool, glass wool and some common AAM precursors. Chemical composition data for soda-lime silicate glasses were obtained from Refs. [13–18] and for glass wools from Refs. [10,11,19,20]. Chemical composition data for stone wools were obtained from Refs. [4,10,11,20–23].

and 7 days.

2.2. Sample characterisation

After curing the hardened samples were demoulded and cut into pieces. With the exception of samples intended for analysis by scanning electron microscopy, the pieces were ground manually using a pestle and mortar and immersed in isopropanol for 25 min to remove loosely bound water and thereby halt the alkali-activation reaction. The ground powders were subsequently filtered prior to storing in a sealed desiccator.

A scanning electron microscope (SEM) [Hitachi TM 3030] with a Bruker Quantax 70 energy-dispersive X-ray spectroscopy (EDX) detector was used to analyse polished cross-sections of the alkali-activated samples. For each sample, the elemental composition was quantified by measuring 70 points across a representative 160 μm × 130 μm section. A 15 keV accelerating voltage and an 8 mm working distance were used.

X-ray diffraction (XRD) data was collected using a Bruker D2 Phaser instrument with Cu Kα radiation, a nickel filter, a step size of 0.020° and 0.5 s/step, and from 5 to 70° 2θ. Phase identification was performed using Diffrac.EVA V3.1 software with the ICDD PDF4+ 2016 database.

Solid state single pulse ^{27}Al and ^{29}Si magic angle spinning (MAS) NMR data were collected with a Bruker Avance III HD 500 spectrometer at 11.7 T (B_0) using a 4.0 mm dual resonance CP/MAS probe, yielding a Larmor frequency of 130.32 MHz for ^{27}Al and 99.35 MHz for ^{29}Si. ^{27}Al MAS NMR spectra were collected with a 1.7 μs non-selective (π/2) excitation pulse, a measured 10 s relaxation delay, a total of 256 transients, and spinning at 12.5 kHz ^{29}Si MAS NMR spectra of the mineral wools were acquired using a 5.5 μs non-selective (π/2) excitation pulse, a measured 30 s relaxation delay, a total of 512 transients and spinning at 12.5 kHz ^{29}Si MAS NMR spectra of the alkali-activated mineral wools were acquired using a 5.5 μs non-selective (π/2) excitation pulse, a measured 45 s relaxation delay, a total of 512 transients and spinning at 12.5 kHz. For all experiments the spectrometer field was aligned to the ^{13}C resonance of adamantane at 38.48 ppm, and ^{27}Al and ^{29}Si spectra were referenced to 1.0 mol/L $Al(NO_3)_3$ in D_2O and tetramethylsilane (TMS), respectively, at 0 ppm.

3. Results and discussion

3.1. Alkali-activated stone wool

3.1.1. SEM-EDX

Backscattered electron (BSE) SEM micrographs of milled stone wool and cross-sections of alkali-activated stone wool are shown in Fig. 2. These micrographs confirm that the milling process destroyed the majority of fibrous nature of stone wool, but some short fibres remained, which is consistent with the fibre length and width data reported in Table 1. There are also some larger particles (~50 μm in diameter) visible in both the precursor and alkali-activated stone wool. Commonly referred to as "shots", these particles are formed during production of stone wool; as much as 16–43 wt% of stone wool may consist of shots [24].

Stone wool activated with $Na_2O{\cdot}2SiO_2$ produced a denser and more homogenous binder than that activated with NaOH (Fig. 2). Porosity of the samples were quantified using image analysis which also confirmed the denser binder of SW $Na_2O{\cdot}2SiO_2$ samples (Supporting information). _There was no distinct change in the binder morphology as observed by SEM imaging of SW_$Na_2O{\cdot}2SiO_2$ between 1 and 7 days of curing, suggesting much of the reaction has occurred within the first 24 h. In contrast, BSE images of the SW_NaOH sample showed clear binder growth during the first 7 days of reaction, indicating slower reaction kinetics when NaOH is used as the activator.

When stone wool is activated with NaOH, binder growth seems to start at the particle surface and then progress outwards (i.e. precipitation begins at nucleation sites on the surface of stone wool particles). In contrast, when activated with $Na_2O{\cdot}2SiO_2$ binder appears evenly dense, suggesting precipitation of the reaction products within the bulk liquid phase with silicate units acting as nucleation sites. Reaction product precipitation from the liquid phase with $Na_2O{\cdot}2SiO_2$ activators and from the surface of precursor particles with NaOH activators has been observed previously in alkali-activated coal fly ash binders [25–28], demonstrating some similarity in the reaction mechanisms occurring with those materials and the mineral wools in this study.

The SEM-EDX data points of NaOH-activated stone wool fall within compositional regions associated with C-(N-)A-S-H and sodium aluminate silicate hydrate (N-A-S-H) gels (Fig. 3). Some SEM-EDX data points also exhibit the bulk composition of stone wool, which is due to the unreacted precursor particles visible in Fig. 2. The presence of stone wool particles also influences the averaged overall composition shown in Fig. 3 to the direction of "Mineral wool" as marked in the diagrams. It is also possible that data points represent a mixture of C-A-S-H and low-Ca C-(N-)A-S-H, or of high-Ca C-(N-)A-S-H and N-A-S-H, if these phases are mixed on a scale smaller than the depth of X-ray generation for the 15 kV accelerating voltage used (<5 μm^3) [27,29]. Between 1 and 7 days of curing there is a minor reduction in the content of Ca in the binder and

Table 2
Mix designs of the alkali activated samples.

Sample name	Stone wool (wt.%)	Glass wool (wt.%)	NaOH (wt.%)	$Na_2O{\cdot}2SiO_2$ (wt.%)	Water/binder[a] (w/w)	Na_2O-dosage of activator (wt.%)[b]
SW_NaOH	67.4	–	32.6	–	0.35	8.0
SW_ $Na_2O{\cdot}2SiO_2$	59.0	–	–	41.0	0.35	8.0
GW_NaOH	–	67.4	32.6	–	0.35	8.0
GW_ $Na_2O{\cdot}2SiO_2$	–	59.0	–	41.0	0.35	8.0

[a] Water to binder ratio. Binder includes mineral wool and all the other components in alkali activator except water.
[b] Na_2O-dosage was 8.0 wt% of the mass of the mineral wool.

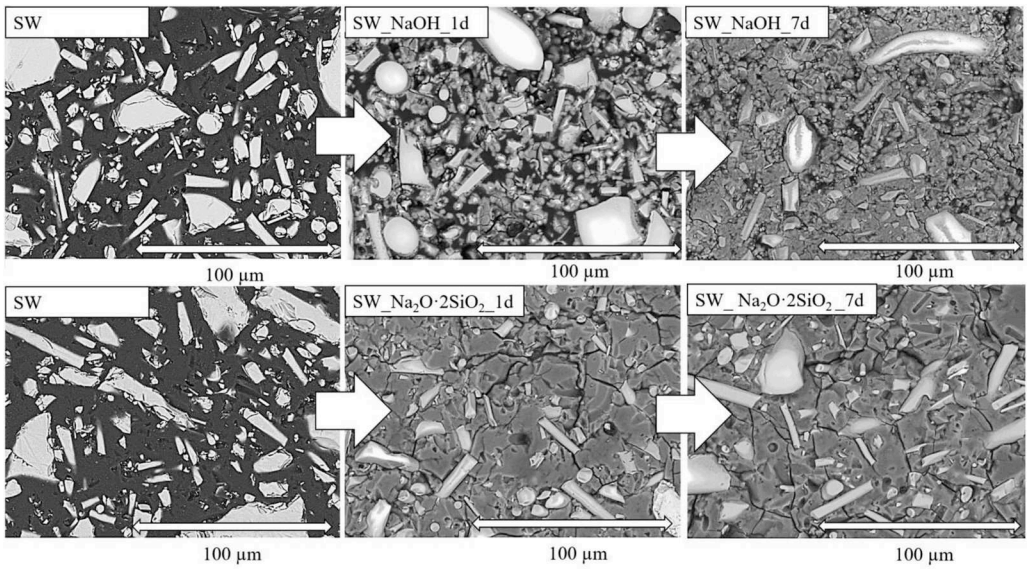

Fig. 2. Back-scattered electron images of milled stone wool in epoxy (SW) and alkali-activated stone wool samples after 1 and 7 days of curing at 40 °C.

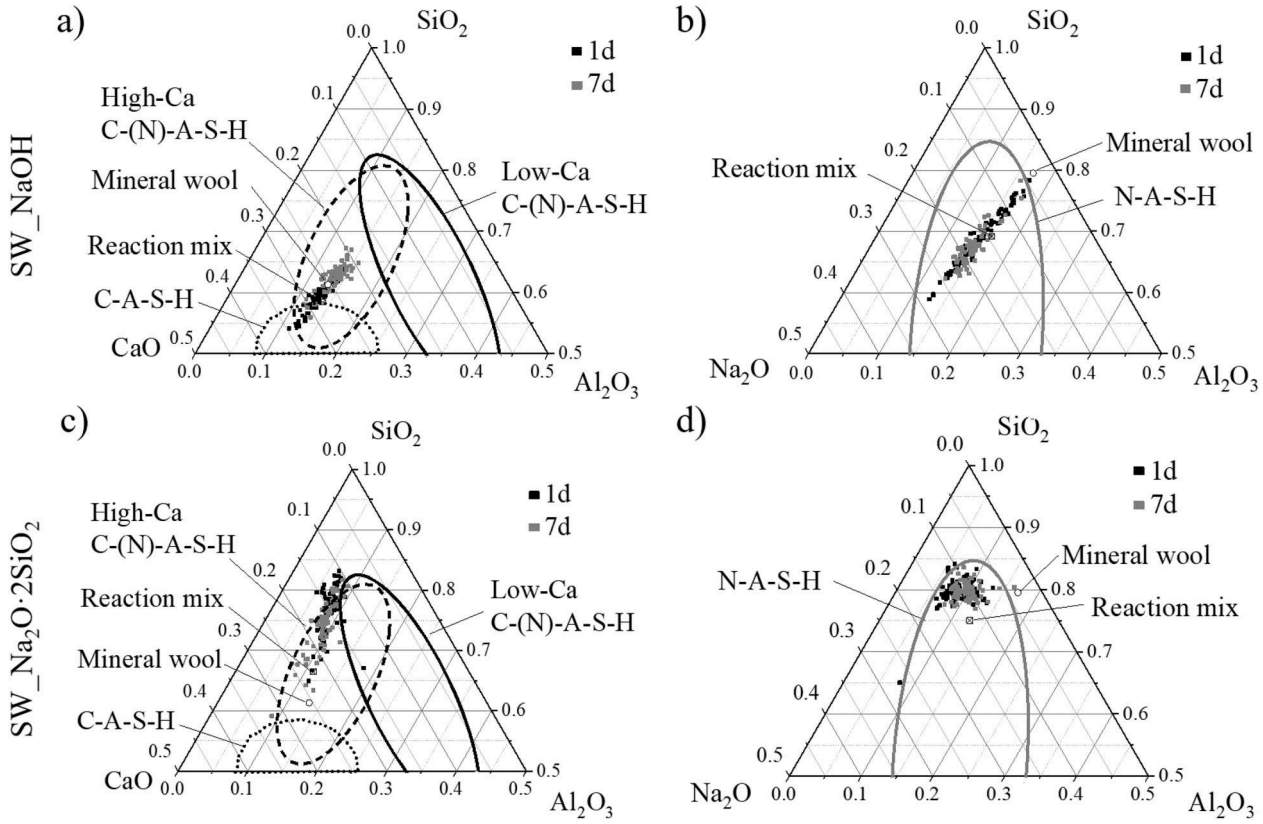

Fig. 3. Diagrams showing the chemical composition as determined by SEM-EDX of SW_NaOH samples in the a) $CaO–SiO_2–Al_2O_3$ and b) $Na_2O–SiO_2–Al_2O_3$ pseudo-ternary systems, and SW_ $Na_2O·2SiO_2$ samples in the c) $CaO–SiO_2–Al_2O_3$ and d) $Na_2O–SiO_2–Al_2O_3$ pseudo-ternary systems, as a function of curing time. Black and grey squares represent the elemental composition after 1 and 7 days of curing, respectively. The areas circled in a) with dotted line, dashed line, and solid black line correspond to C-A-S-H gel, high-Ca C-(N-)A-S-H and low-Ca C-(N-)A-S-H gels respectively, as determined in Refs. [30,31]. The area circled with the grey solid line in b) corresponds to a N-A-S-H gel as determined in Refs. [32,33]. Mineral wool composition was determined by SEM-EDX whereas the composition of the reaction mixture was calculated from the precursor composition as determined by XRF from the activator compositions. Note: For clarity the diagram shows CaO and Al_2O_3 content up to a maximum of 0.5.

consequently a minor increase in the content of Si and Al. This suggests incongruent dissolution of the precursor; preferential dissolution of Ca from the precursor results in a binder that is initially Ca-rich, with subsequent dissolution of Si and Al from the precursor resulting in their incorporation into the binder.

SEM-EDX data indicate that the main reaction product of $Na_2O·2SiO_2$-activated stone wool is C-(N-)A-S-H gel or a mixture of both high-Ca and low-Ca C-(N-)A-S-H and N-A-S-H gels, similar to NaOH-activated stone wool, but with lower Ca and higher Si content. This is expected due to the additional Si in the alkali activator. There is a slight

change in the binder chemical composition over time; the content of Ca and Al increases and content of Si decreases. The binder formation likely results from reaction product precipitation in the liquid phase, with from silicate units acting as nucleation centres, resulting in an initially high concentration of Si within the binder as reported in sodium silicate-activated coal fly ash and GGBFS mixes [25–28]. Further precursor dissolution then releases more Ca and Al which are incorporated into the binder structure.

3.1.2. XRD

The main reaction product of NaOH- and $Na_2O{\cdot}2SiO_2$-activated stone wool is X-ray amorphous (Fig. 4). Typically, disordered N-A-S-H and C-(N-)A-S-H phases exhibit a broad feature at approximately 29° 2θ [34]. A broad feature with a sharper, small peak at its centre is visible in the X-ray diffractograms of NaOH-activated samples, consistent with the structure of Al-substituted tobermorite (PDF # 19–0052). This indicates the presence of C-(N-)A-S-H, consistent with the SEM-EDX data discussed above, although the peak overlaps with the most intense peak from calcite ($CaCO_3$, PDF #04-012-0489) at 29.3° 2θ and so the presence of that phase cannot be determined unambiguously from the XRD data alone.

Low intensity reflections due to the Mg LDH phase quintinite ($Mg_4Al_2(OH)_{12}CO_3{\cdot}3H_2O$, PDF #00-051-1528) and zeolite F ($Na_5Al_5Si_5O_{20}{\cdot}9H_2O$, PDF #04-017-7268) (for which only the reflections at 11.8 and 23.5° 2θ for Mg-LDH and at 12.4 and 28.2° 2θ for zeolite F) were observed. Additionally, carbonate phases thermonatrite, ($Na_2CO_3{\cdot}H_2O$, PDF #00-008-0448 and calcite ($CaCO_3$, PDF #04-012-0489), were observed in NaOH-activated stone wool. The formation of quintinite results from the relatively high levels of MgO in stone wool (compared with other glassy AAM precursors such as GGBFS and fly ash [35–37]), while the formation of zeolite phases is common in alkali activation of low-Ca precursors [38]. The formation of the carbonate phases is most likely a result of sample carbonation during exposure to atmospheric CO_2 during preparation for analysis. None of the crystalline phases (quintinite, zeolite F or the carbonate phases) are observed in the SEM-BSE images or EDX data, indicating that these phases either occupy a volume of less than $< 5\ \mu m^3$ or are present in such low concentrations as to be unobservable in the final averaged data.

No difference is observed in the XRD data for $Na_2O{\cdot}2SiO_2$-activated stone wool cured for 1 and 7 days (consistent with the SEM-EDX data discussed above). The only difference in the XRD data for NaOH-activated stone wool cured for 1 and 7 days observable in the XRD data is the absence of reflections due to thermonatrite in the data this sample cured for 7 days. This could be due to differences in exposure to atmospheric CO_2 during sample preparation, or thermonatrite may be present in the sample cured for 7 days in a low amount such that any reflections due to this phase are not observable above the noise in the XRD data.

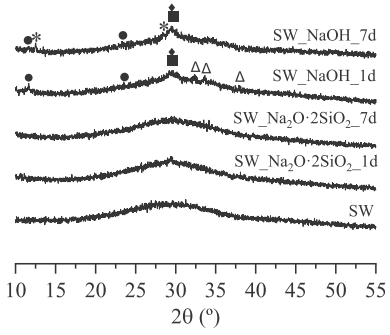

Fig. 4. X-ray diffractograms of anhydrous stone wool (SW) and NaOH- and $Na_2O{\cdot}2SiO_2$-activated stone wool cured for 1 and 7 days. Symbols: Δ: thermonatrite, $Na_2CO_3{\cdot}H_2O$; ◆: calcite, $CaCO_3$; ●: quintinite, $Mg_4Al_2(OH)_{12}CO_3{\cdot}3H_2O$; *: zeolite F (Na), $Na_5Al_5Si_5O_{20}{\cdot}9H_2O$; ■: C-(N-)A-S-H.

3.1.3. NMR

The ^{27}Al and ^{29}Si MAS NMR spectra of anhydrous and alkali activated stone wool are shown in Fig. 5. Anhydrous stone wool comprises a single large distribution of Al and Si sites, consistent with the glassy nature of the mineral wool. Al exists in predominantly tetrahedral coordination (indicated by the maximum of the distribution at $\delta_{obs} = -59$ ppm), with significant quantities of pentahedral and octahedral coordinated Al sites (Fig. 5 a). The ^{29}Si MAS NMR spectrum of anhydrous stone wool exhibits a large distribution of resonances spanning from $\delta_{iso} = -60$ ppm to -130 ppm; this region is associated with all $Q^n(m\text{Al})$ species ($0 \leq m \leq n \leq 4$) in the glass that forms during the rapid quenching of molten stone wool that occurs as fibres are spun during manufacturing [39]. The distribution is centred at approximately $\delta_{iso} = -90$ ppm, indicating that the most populous Si species is either $Q^3(1Al)$ or $Q^4(4Al)$, or a combination of these.

3.1.3.1. ^{27}Al MAS NMR of alkali-activated stone wool. Alkali-activation of stone wool with $Na_2O{\cdot}2SiO_2$ results in a significant narrowing of the distribution in the ^{27}Al MAS NMR spectrum, which is now centred at $\delta_{obs} = 61.4$ ppm and extends from $\delta_{obs} = 80$ ppm to 40 ppm. This indicates the formation of a new distribution of tetrahedral Al environments which is significantly more ordered than that observed in anhydrous stone wool, albeit still exhibiting an extensive distribution of chemical shifts (and hence indicating extensive disorder). The position and width of the new distribution of tetrahedral Al resonances is consistent with tetrahedral Al within disordered C-(N-)A-S-H or N-A-S-H gels [37,40]. The large distribution of chemical shifts indicates extensive disorder and a large distribution of Al–O–Si bond angles in these gels. No further change is observed in the ^{27}Al MAS NMR spectrum (and therefore Al environments) of stone wool activated with sodium silicate and cured for 7 days, consistent with the SEM observations discussed above.

Alkali-activation of stone wool with NaOH also results in a significant narrowing of the distribution in the ^{27}Al MAS NMR spectrum (now extending from $\delta_{obs} = 80$ ppm to 30 ppm and centred at $\delta_{obs} = 65.1$ ppm). Again, this indicates the formation of a new distribution of tetrahedral Al environments that is significantly more ordered than that observed for anhydrous stone wool, indicative of tetrahedral Al within C-(N-)A-S-H or N-A-S-H gels [37,40]. The distribution of Al^{IV} sites in

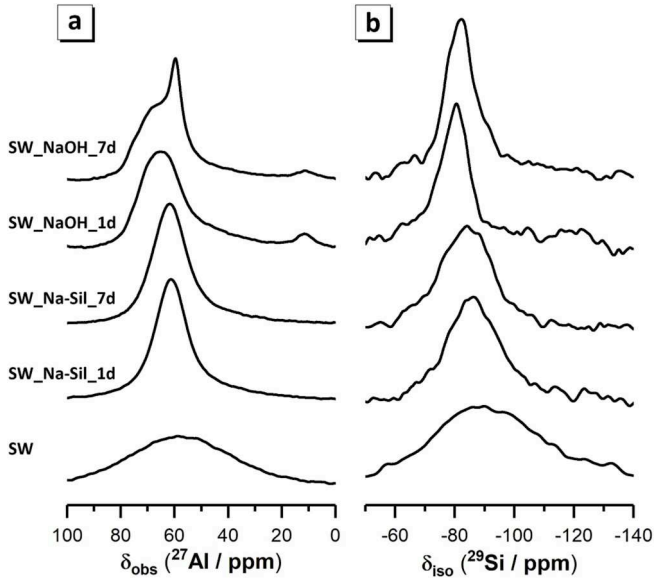

Fig. 5. a) ^{27}Al MAS (12.5 kHz) NMR spectra and b) ^{29}Si MAS (12.5 kHz) NMR spectra of anhydrous and alkali-activated stone wool, cured for 1 day and 7 days at 40 °C as marked.

stone wool activated by NaOH is significantly deshielded compared with that of stone wool activated by $Na_2O{\cdot}2SiO_2$, resulting in the distribution shifting towards higher chemical shift values, indicating a decrease in the surrounding electron density, and therefore a lower Si/Al ratio in the C-(N-)A-S-H or N-A-S-H gels. There is also a small shoulder on this resonance at approximately $\delta_{obs} = 46$ ppm due to the presence of Al in pentahedral environments. Alkali-activation is not expected to result in formation of such disordered environments, and as such the pentahedral Al may be attributed to remnant anhydrous stone wool within the binder matrix. This suggests slower reaction kinetics when stone wool is activated with NaOH compared with $Na_2O{\cdot}2SiO_2$. A sharp resonance is centred at $\delta_{obs} = 60.0$ ppm is observed in the ^{27}Al MAS NMR spectrum of stone wool activated with NaOH and cured for 7 days, indicating the formation of a new tetrahedral Al environment (possibly the zeolite F phase identified by XRD) exhibiting significantly more order than was formed in the initial stages of reaction. A low intensity, sharp resonance (relative to the broad Al^{IV} resonance) is also observed at $\delta_{obs} = 12$ ppm, consistent with the chemical shift at which Al^{VI} sites in Mg-rich LHD phases from the hydrotalcite family resonate. This resonance is therefore attributed to Al^{VI} sites within quintinite ($Mg_4Al_2(OH)_{12}CO_3{\cdot}3H_2O$), consistent with identification of this phase in the XRD data above.

3.1.3.2. ^{29}Si MAS NMR of alkali-activated stone wool. A narrowing of the distribution of chemical shift values in the ^{29}Si MAS NMR spectrum is observed upon alkali-activation of stone wool with $Na_2O{\cdot}2SiO_2$. Difference ^{29}Si MAS NMR spectra for each alkali-activated stone wool (Fig. 6) provide information about the net consumption (indicated by regions of negative intensity) and net production (indicated by regions of positive intensity) of different Si species during alkali-activation.

Upon alkali activation of stone wool with $Na_2O{\cdot}2SiO_2$ there is a net production of Q^2 and Q^2(1Al) species ($\delta_{iso} = -85$ and -80, respectively), driven by a net consumption of precursor Q^0, Q^1 and Q^n(*m*Al) ($n = 3$ or 4, $m = 0$–4) Si sites during reaction. The net production of Q^2 and Q^2(1Al) species indicates formation of a C-(N-)A-S-H gel [37,40,41].

Significant intensity is also observed at approximately -90 to -100 ppm in the ^{29}Si MAS NMR spectrum of stone wool activated with $Na_2O{\cdot}2SiO_2$ (Fig. 5 b). Intensity in this region can be attributed to the presence of either crosslinking Q^3(1Al) and Q^3 species within C-(N-)A-S-H [42,43] or fully polymerised Q^4(4Al) and Q^4(3Al) species within N-A-S-H [34,37,44], or a combination of both. It is also possible that the intensity in this region is due to resonances from these Si species in anhydrous stone wool, however this would require preferential dissolution of low-Al substituted fully polymerised Q^4 species and low-polymerisation Q^1 species during alkali-activation. As anhydrous stone wool is completely X-ray amorphous and shows extensive disorder in its ^{29}Si MAS NMR spectrum, such extensive incongruent dissolution is unlikely to be occurring. The congruency of the dissolution was estimated using BSE-image analysis and EDX data which confirmed that the dissolution is near-congruent (Supporting information). Therefore, the intensity in this region must be assigned to species in either C-(N-)A-S-H or N-A-S-H reaction products.

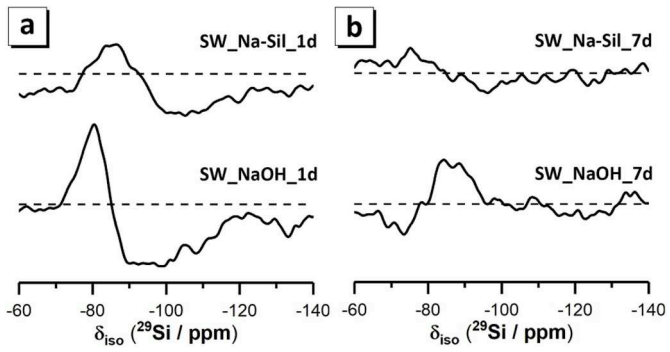

Fig. 6. Difference plots generated by: a) subtracting the ^{29}Si MAS NMR spectrum of stone wool from that of alkali-activated stone wool cured for 1 day; and b) subtracting the ^{29}Si MAS NMR spectrum of alkali-activated stone wool cured for 1 day from that of alkali-activated stone wool cured for 7 days. Baselines are indicated by the grey dotted lines.

Alkali activation of stone wool with NaOH results in a net production of primarily Q^2(1Al) species ($\delta_{iso} = -80$), with net consumption of precursor Q^0, Q^1, Q^2 and Q^n(*m*Al) ($n \geq 3$, $m \geq 0$) Si sites during reaction, indicating formation of a C-(N-)A-S-H gel with greater inclusion of Al within the aluminosilicate chains (consistent with the decrease in Si/Al ratio of the C-(N-)A-S-H gel observed by ^{27}Al MAS NMR). Greater Al incorporation within C-(N-)A-S-H in stone wool activated by NaOH can be attributed to the lower amount of freely available Si ions within the reaction mixture, due to the absence of a source of soluble silica in the activating solution. Q^2 and Q^2(1Al) species present within stone wool will also be consumed during alkali-activation, however this is not reflected by negative intensity within the region of these resonances in Fig. 6, suggesting that the amount of new Q^2 and/or Q^2(1Al) Si species produced during alkali-activation is likely to be significantly higher than is indicated by the net positive intensity these regions. Intensity within the -90 to -100 ppm region of the ^{29}Si MAS NMR spectrum of stone wool activated with NaOH cured for 1 day is negligible, suggesting that a N-A-S-H-type gel has not formed in this sample, likely due to the absence of soluble silica in the activation solution and subsequent limitations on freely available Si.

After 7 days' curing the ^{29}Si MAS NMR spectrum of stone wool activated by $Na_2O{\cdot}2SiO_2$ exhibited an increase in intensity in the region attributed to Q^2(1Al) Si sites ($\delta_{iso} = -80$) compared with that of stone wool activated with $Na_2O{\cdot}2SiO_2$ and cured for 1 day. This indicates that as the reaction progresses, increased amounts of Al are incorporated into the aluminosilicate chains of C-(N-)A-S-H in stone wool activated with $Na_2O{\cdot}2SiO_2$, due to depletion of the higher amount of soluble Si in the initial stages of reaction (which promoted formation of Q^2 Si species), and subsequent dissolution of Al from the stone wool precursor. This explanation is again supported by the additional data presented as Supporting Information which shows that the Si/Al molar ratio of the binder gel decreases as the reaction progresses.

In contrast, after 7 days' curing the ^{29}Si MAS NMR spectrum of stone wool activated by NaOH exhibited an increase in intensity in the region attributed to Q^2 Si sites ($\delta_{iso} = -85$ ppm) compared with that of the corresponding sample cured for 1 day. This is due to the lower amount of soluble Si present in the initial stages of reaction (which promoted formation of Q^2(1Al) in addition to Q^2 species) compared to stone wool activated with $Na_2O{\cdot}2SiO_2$, and subsequent dissolution of Si from the stone wool precursor and incorporation into the C-(N-)A-S-H gel. This demonstrates that the reaction kinetics and gel composition can be controlled by adjusting the activating solution chemistry.

3.1.4. Discussion of stone wool-based binders

SEM-EDX, XRD and NMR data show that the main binding phase formed in NaOH-activated stone wool is an X-ray amorphous C-(N-)A-S-H-type gel, which is broadly comparable to those identified in alkali-activated GGBFS binders but displays greater disorder. The gel chemical composition is initially Ca- and Al-rich, and evolves during the curing period to incorporate more Si as the reaction progresses, as shown by SEM-EDX and NMR data. The degree of cross-linking of the C-(N-)A-S-H gel (i.e. the content of Q^3 and Q^3 (1Al)) is relatively low in the SW_NaOH sample.

The Mg-rich LDH phase quintinite ($Mg_4Al_2(OH)_{12}CO_3{\cdot}3H_2O$) and zeolite F ($Na_5Al_5Si_5O_{20}{\cdot}9(H_2O)$ also form as an additional reaction products in the SW_NaOH sample (identified by XRD). Formation of different types of Mg- and Al-containing LDH phases from the broader hydrotalcite family, including quintinite, depends on the Mg/Al ratio, carbonate and water content, and temperature [45]. The main difference between true hydrotalcite and quintinite group members is the Mg:Al ratio, with quintinite exhibiting a Mg:Al ratio of 2:1 and hydrotalcite

exhibiting a Mg:Al ratio of 3:1 [45]. The role of Mg in AAM is of particular interest since alkali-activated GGBFS with varying MgO content (1.1–7.5 wt%) showed improved carbonation resistance as a function of bulk MgO content, as hydrotalcite acts as an internal CO_2 sorbent [35]. Alkali-activated slags with MgO content above 5 wt% form hydrotalcite in addition to the main C-A-S-H gel reaction product. Additionally, higher slag MgO content promotes a greater extent of reaction and reduced Al incorporation in the C-A-S-H. The stable coexistence of Mg-rich LDH phases and the main C-(N-)A-S-H gel reaction product in NaOH-activated stone wool suggests that the reaction kinetics may be controlled further by addition of calcined layered double hydroxides [46].

Zeolite F was identified in SW_NaOH sample after 7 days of curing. This type of zeolite has the edingtonite-type framework structure and is built from $Al_2Si_3O_{10}$ chains similar to those found in natrolite. However, the tetrahedra are bound to neighbouring chains with no translation parallel to *c* [47]. Formation of zeolite F is rare in Ca-rich alkali-activated binders, but it has been observed in binders produced from coal fly ash activated with 6 M NaOH which were seeded with Al_2O_3 nanoparticles (forming in the regions of Al-rich gel that have the correct stoichiometry) [25]. Formation of zeolite phases is common in alkali-activated binders based on low-Ca precursors such as metakaolin and fly ash [38].

SEM-EDX, XRD and NMR data show that the main binding phase formed in $Na_2O{\cdot}2SiO_2$-activated stone wool is an X-ray amorphous C-(N-)A-S-H-type gel containing low Ca content, which is again broadly comparable to those identified in alkali-activated GGBFS binders but displays greater disorder. The presence of soluble Si in the activator results in a gel that is initially rich in Si, with greater amounts of Ca and Al being incorporated in the gel as the reaction progresses.

The presence of either crosslinking Q^3(1Al) and Q^3 species within C-(N-)A-S-H [42,43] or fully polymerised Q^4(4Al) and Q^4(3Al) species within N-A-S-H [34,37,44], or a combination of both, was observed in the ^{29}Si MAS NMR data for stone wool activated with $Na_2O{\cdot}2SiO_2$. C-A-S-H and C-(N-)A-S-H gels in hydrated PC/slag blends, alkali-activated slags and synthetic gels (as a close point of comparison) typically exhibit Ca/Si ratios of between 1.0 and 1.6 [43,48–50], and phase-pure C–S–H forms a continuous structural series with Ca/Si ratios between 0.55 and 2.0 [51–53]. Assuming then that all Ca within stone wool is dissolved during alkali-activation and are incorporated into a C-(N-)A-S-H gel with $0.55 \leq Ca/Si \leq 2.0$ and $Al/Si = 0.1$, there will be more freely available Al than can be incorporated into a C-(N-)A-S-H gel (the limitation arises from the structural limitations described by the cross-linked substituted tobermorite model for C-(N-)A-S-H [42]).

Therefore, at least some of the intensity in the −90 to −100 ppm region in the ^{29}Si MAS NMR spectrum of stone wool activated with $Na_2O{\cdot}2SiO_2$ (discussed above) must be attributed to a fully polymerised Q^4(4Al) and Q^4(3Al) species within an Al-rich N-A-S-H type gel. This indicates that alkali-activation of stone wool with $Na_2O{\cdot}2SiO_2$ drives formation of a low-Ca C-(N)-A-S-H gel with maximum Al and Na incorporation that is thermodynamically stable [42,54], with excess alkali and freely available Si and Al driving formation of an additional Al-rich N-A-S-H gel reaction product, possibly including nanocrystalline zeolite precursors that do not give a sharp XRD peak [38]. This analysis is further supported by the fact that the activating solution provides ample freely available soluble Si for formation of an additional Al-rich N-A-S-H gel.

The dense microstructure of the SW_$Na_2O{\cdot}2SiO_2$ binder that formed after curing for 1 day indicates that additional soluble Si species provided by the $Na_2O{\cdot}2SiO_2$ activating solution accelerate the reaction kinetics and hardening of the binder significantly compared to activation with NaOH. With both activators stone wool dissolution is likely to not be fully congruent, as discussed in the Supporting Information where BSE-image analysis, XRF and EDX data was used to study the dissolution rate. The differentiation between the use of NaOH and $Na_2O{\cdot}2SiO_2$ activators in promoting hydration products, and filling space, can be anticipated from the greater availability of soluble silica [55]. The higher pH of NaOH can affect the reactivity of the hydrated alkaline earth ions [55] which may account for precipitation of the Mg-bearing phase (quintinite) and the presence of zeolites arising in the present study. As mentioned in Section 2.1, to obtain a clear understanding of the dissolution and gel formation mechanisms of the aluminosilicate phases in mineral wool waste, the mineral wools used in this study to not contain organic resin coatings. Actual mineral wool waste contains organic resin coatings which could affect both the dissolution process and gel formation mechanism.

3.2. Alkali-activated glass wool

3.2.1. SEM-EDX

Backscattered electron SEM micrographs showing milled glass wool and cross-sections of alkali-activated glass wool binders are shown in Fig. 7. The micrographs show that milling process destroyed the fibrous nature of glass wool effectively. Only short (<30 μm in length) fibres are visible by SEM, which is consistent with the fibre length and width measurements presented in Table 1. Fibres are evenly distributed in the binder matrix and appear to be randomly oriented.

The binder formed with NaOH activated glass wool densifies visibly between 1 and 7 days curing, indicating progressive hardening reactions during this period (Fig. 7). Activation with $Na_2O{\cdot}2SiO_2$ produces a denser binder microstructure after 1 day of curing, and no significant change in the binder matrix density or morphology is visible with further curing. All glass wool-based samples have microcracks in the binder, indicating loss of water during hardening, sample pre-treatment, and/or when exposed to the low-vacuum conditions of SEM.

Chemical composition data obtained via SEM-EDX (Fig. 8) indicate that the alkali-activated glass wool binder is a sodium silicate gel with low amounts of Ca and Al. As discussed earlier some SEM-EDX data points also exhibit the bulk composition of glass wool, which is due to the unreacted precursor particles visible in Fig. 7. The presence of glass wool particles slightly changes the overall composition shown in Fig. 8 to the direction of "Mineral wool" as marked in the diagrams. The chemical composition of the glass wool-based binders is dependent on the activator used, with $Na_2O{\cdot}2SiO_2$ (which provides a source of soluble Si) resulting in greater gel Si content than NaOH.

Little difference is observed in the binder chemical composition of $Na_2O{\cdot}2SiO_2$-activated glass wool between 1 and 7 days, suggesting much of the reaction has occurred within the first 24 h. However, the binder chemical composition of NaOH-activated glass wool indicates that the gel is Si rich during the early stages of reaction (first 24 h) and subsequently incorporates greater Na content after 7 days.

The measured content of Na in the binders is lower than that of the reaction mix in all data points. SEM-EDX may give lower than expected content of Na [29] due to possible removal of Na during sample preparation and polishing, and thus it is possible that the as-synthesised gel has higher Na content than shown in Fig. 8.

3.2.2. XRD

The main reaction product in both NaOH- and $Na_2O{\cdot}2SiO_2$-activated glass wool is X-ray amorphous (Fig. 9), consistent with the formation of a sodium silicate glass and the chemical composition identified by SEM-EDX. A broad feature with a sharper, small peak at its centre is visible in the X-ray diffractograms of NaOH-activated samples (similar to that observed in NaOH-activated stone wool). In NaOH-activated stone wool this sharper, small peak at approximately 29° 2θ was attributed to either a C-(N-)A-S-H type gel displaying structural similarity with Al-substituted tobermorite (PDF # 19–0052), calcite ($CaCO_3$, PDF #04-012-0489) or a combination of both phases.

Glass wool contains significantly lower amounts of CaO (8.2 wt% c.f. 15.3 wt% for stone wool) and as such the formation of both C-(N-)A-S-H type gels and calcite is expected to be minimal. Previous work has shown that N-A-S-H gels can incorporate up to 10 mol. % of Ca into the gel

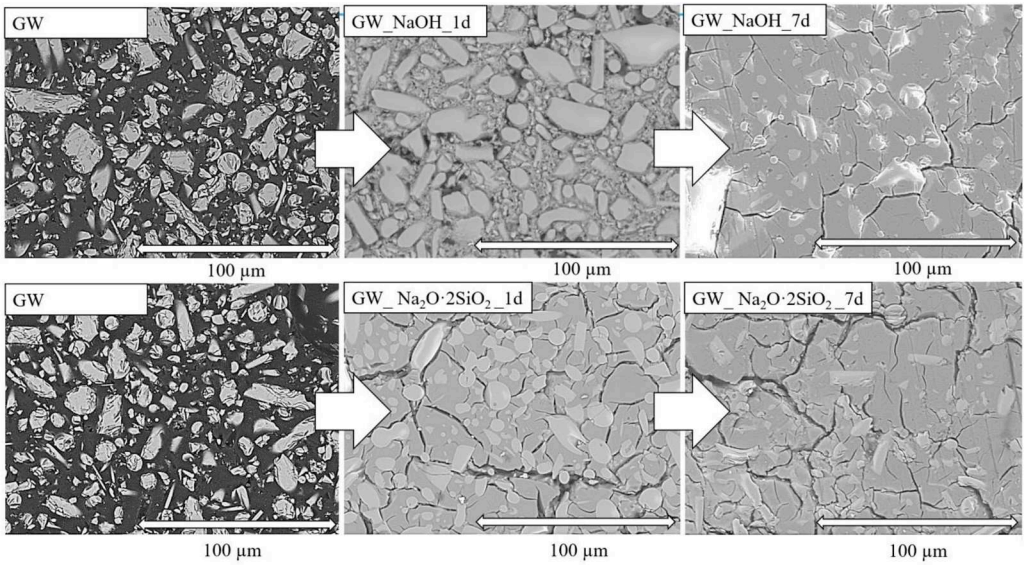

Fig. 7. Back-scattered electron images of milled glass wool (GW) in epoxy and alkali-activated glass wool samples after 1 and 7 days of curing at 40 °C.

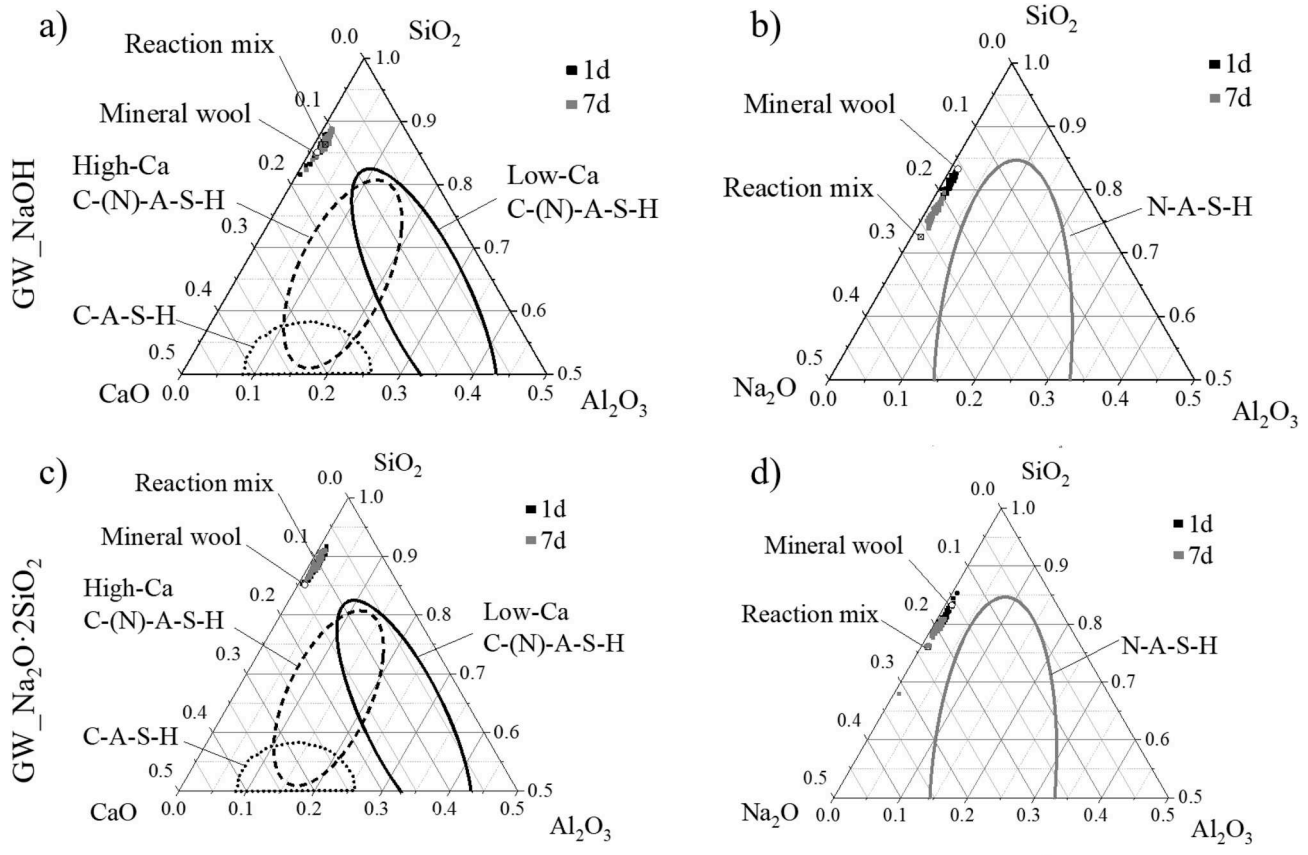

Fig. 8. Diagrams showing the chemical composition as determined by SEM-EDX of GW_NaOH samples in the a) $CaO–SiO_2–Al_2O_3$ and b) $Na_2O–SiO_2–Al_2O_3$ pseudo-ternary systems, and GW_ $Na_2O·2SiO_2$ samples in the c) $CaO–SiO_2–Al_2O_3$ and d) $Na_2O–SiO_2–Al_2O_3$ pseudo-ternary systems, as a function of curing time. Black and grey squares represent the elemental composition after 1 and 7 days of curing, respectively. The areas circled in a) with dotted line, dashed line, and solid black line correspond to C-A-S-H gel, high-Ca C-(N-)A-S-H and low-Ca C-(N-)A-S-H gels, respectively, as determined in Refs. [30,31]. The area circled with the grey solid line in b) corresponds to a N-A-S-H gel as determined in Refs. [32,33]. Mineral wool composition was determined by SEM-EDX whereas the composition of the reaction mixture was calculated from the precursor composition as determined by XRF from the activator compositions.

framework, forming a partially Ca-substituted N-A-S-H (N-(C-)A-S-H) type gel [30], and it is therefore more likely, from simple stoichiometric arguments, that a partially Ca- and Al-substituted sodium silicate glass phase will form in the alkali-activated glass wool systems here. The type of gel formed cannot be determined unambiguously from the XRD data alone (although the SEM-EDX data indicates formation of a reaction

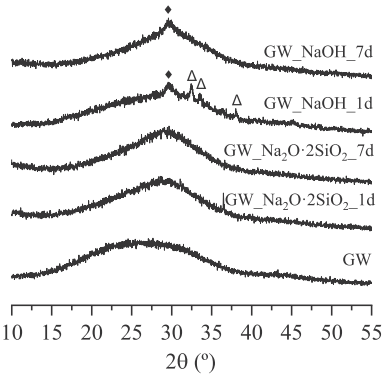

Fig. 9. X-ray diffractograms of the anhydrous glass wool and NaOH- and $Na_2O{\cdot}2SiO_2$-activated glass wool cured for 1 and 7 days at 40 °C. Nomenclature: Δ: thermonatrite, $Na_2CO_3{\cdot}H_2O$; ◆: calcite, $CaCO_3$.

product with chemistry consistent with a sodium silicate glass), however this will be revisited in detail during discussion of the NMR data below.

Thermonatrite ($Na_2CO_3{\cdot}H_2O$, PDF #00-008-0448) was also identified in NaOH-activated glass wool, again formed as a result of sample carbonation during exposure to atmospheric CO_2 during preparation for analysis. In the GW_$Na_2O{\cdot}2SiO_2$_1d sample a peak at 36° 2θ is tentatively attributed fayalite (Fe_2SiO_4, which exhibits its largest reflection at 36° 2θ), resulting from minor contamination during sample preparation, however the identification is not certain as it is based on a single reflection. As with alkali-activated stone wool, none of the carbonate phases identified by XRD are observed in the SEM-BSE images or EDX data. This may be due to the fact that these phases occupy a volume of less than <5 μm^3, or that they are present in such low concentrations as to be unobservable in the final averaged data.

Similar to alkali-activated stone wool, no difference is observed in the XRD data for $Na_2O{\cdot}2SiO_2$-activated glass wool cured for 1 and 7 days (consistent with the SEM-EDX data discussed above), and the only difference in the XRD data for NaOH-activated stone wool cured for 1 and 7 days observable in the XRD data is the absence of reflections due to thermonatrite in the data this sample cured for 7 days. This is again attributed to differences in exposure to atmospheric CO_2 during sample preparation, or the presence of thermonatrite in the sample cured for 7 days in a such low amounts that any reflections due to this phase are not observable above the noise in the XRD data.

3.2.3. NMR

^{27}Al and ^{29}Si MAS NMR spectra for anhydrous and alkali activated glass wool are shown in Fig. 10. Similar to stone wool, anhydrous glass wool comprises a single large distribution of Al and Si sites, consistent with the glassy nature of the mineral wool. Al exists in predominantly tetrahedral coordination (indicated by the maximum of the distribution at $\delta_{obs} = -57$ ppm), with significant quantities of pentahedral but no octahedral Al sites (Fig. 5a). The ^{29}Si MAS NMR spectrum of anhydrous glass wool exhibits a large distribution of resonances spanning from $\delta_{iso} = -70$ ppm to −120 ppm, centred at $\delta_{iso} = -91$ ppm, that is likely to contain contributions from a wide range of $Q^n(m\text{Al})$ species that form during the rapid quenching of molten glass wool that occurs as fibres are spun during manufacturing [39]. The distribution is centred at approximately $\delta_{iso} = -90$ ppm, indicating that the most populous Si species is either Q^3(1Al) or Q^4(4Al), or a combination of these (similar to that observed for anhydrous stone wool).

3.2.3.1. ^{27}Al MAS NMR of alkali-activated glass wool. As with stone wool, alkali-activation of glass wool with $Na_2O{\cdot}2SiO_2$ results in a significant narrowing of the ^{27}Al MAS NMR distribution (now centred at $\delta_{obs} = 59.0$ ppm), indicating formation of a new, more ordered distribution of tetrahedral Al environments in a newly formed reaction

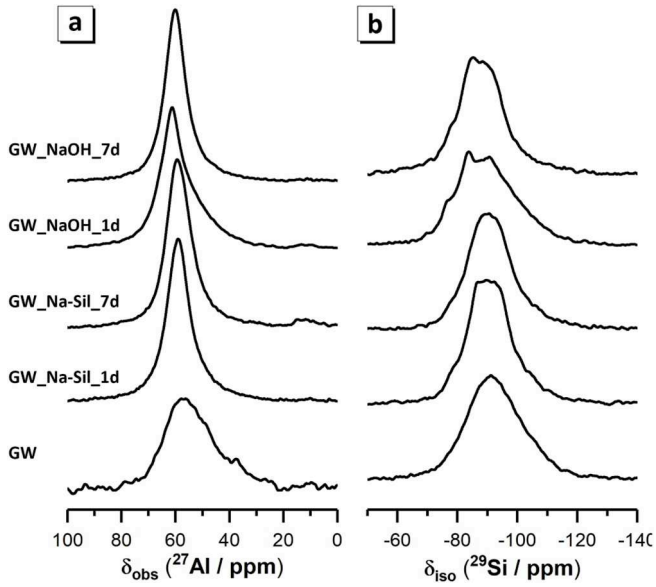

Fig. 10. a) ^{27}Al MAS (12.5 kHz) NMR, and b) ^{29}Si MAS (12.5 kHz) NMR spectra of anhydrous and alkali-activated glass wool, cured for 1 day and 7 days as marked.

product. The large distribution of chemical shifts indicates extensive disorder and a large distribution of Al–O–Si bond angles in these gels. No further change is observed in the ^{27}Al MAS NMR spectrum of glass wool activated with $Na_2O{\cdot}2SiO_2$ and cured for 7 days, consistent with the observations from SEM and XRD data discussed above.

Alkali-activation of glass wool with NaOH also results in a sharpening of the distribution in the ^{27}Al MAS NMR spectrum (now centred at $\delta_{obs} = 61.0$ ppm), also indicating the formation of a new, more ordered distribution of tetrahedral Al environments in a newly formed reaction product. The slight deshielding of this distribution of Al^{IV} sites in glass wool activated by NaOH compared to that of glass wool activated by $Na_2O{\cdot}2SiO_2$ indicates a lower Si/Al ratio in this new reaction product. There is also a large shoulder on this resonance towards lower chemical shift values. The lineshape of this shoulder is consistent with that of anhydrous glass wool, suggesting the presence of remnant anhydrous glass wool particles within the binder matrix and slower reaction kinetics when glass wool is activated by NaOH compared with $Na_2O{\cdot}2SiO_2$. This is again consistent with the observations from SEM and XRD data for stone wool discussed above. After curing for 7 days, the ^{27}Al MAS NMR spectrum of glass wool activated by NaOH exhibits a lineshape almost identical to that of glass wool activated with $Na_2O{\cdot}2SiO_2$.

The small quantity of Al within glass wool (1.5 wt %) and overall stoichiometry of the reaction mixture and resultant binder for alkali-activated glass wool suggests that these Al^{IV} sites exist within an Al-substituted sodium silicate reaction product.

3.2.3.2. ^{29}Si MAS NMR of alkali-activated glass wool. A narrowing of the distribution of chemical shift values in the ^{29}Si MAS NMR spectrum is observed upon alkali-activation of glass wool by $Na_2O{\cdot}2SiO_2$. Difference ^{29}Si MAS NMR spectra for each alkali-activated glass wool (Fig. 11) show that, upon alkali activation of glass wool with $Na_2O{\cdot}2SiO_2$, there is a net production of Si species with chemical shifts in the range $\delta_{iso} = -82$ ppm to −97 ppm. Considering the low Al content within glass wool (1.5 wt %), this intensity is likely to be primarily due to Q^2 or Q^3 species in an amorphous sodium silicate phase, similar to those previous observed in sodium silicate glasses [56]. ^{29}Si MAS NMR spectrum of glass wool activated with $Na_2O{\cdot}2SiO_2$ and cured for 7 days exhibits a slight decrease in intensity in the region $\delta_{iso} = -83$ to −97 ppm and a slight increase in intensity in the region $\delta_{iso} = -100$ to −110 ppm,

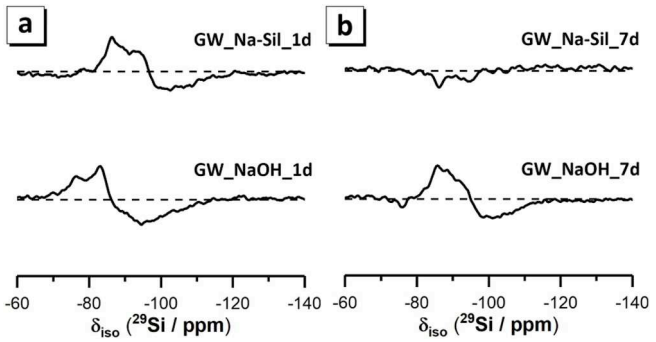

Fig. 11. Difference plots generated by a) subtracting the ^{29}Si MAS NMR spectrum of glass wool from that of alkali-activated glass wool cured for 1 day and b) subtracting the ^{29}Si MAS NMR spectrum of alkali-activated glass wool cured for 1 day from that of alkali-activated glass wool cured for 7 days. Baselines are indicated by the grey dotted lines.

suggesting increased polymerisation as the reaction progresses.

The presence of 8.2 wt % CaO in glass wool means that it is likely that a partially Ca- and Al-substituted sodium silicate type gel (N-(C-)(A-)S–H) has also formed in GW_$Na_2O{\cdot}2SiO_2$, aligning with the observation of tetrahedral Al resonances in the ^{27}Al MAS NMR spectra of alkali-activated glass wool. This gel contains Q^1, Q^2, Q^2(1Al) and possibly Q^3 sites (in addition to which will contribute to the intensity in the range $\delta_{iso} = -75$ ppm to -97 ppm [37,40,41].

Alkali activation of glass wool with NaOH results in a net production of primarily Q^1, Q^2, and Q^2(1Al) species ($\delta_{iso} = -77$ to -83), with net consumption of precursor Q^3 and Q^4 species during reaction. As with glass wool activated by $Na_2O{\cdot}2SiO_2$, this is consistent with the formation of an amorphous sodium silicate phase similar to those previously observed in sodium silicate glasses [56] and the N-(C-)(A-)S–H type gel identified above. Further production of Q^2 and Q^3 species and consumption of Q^4 species occurs as the reaction progresses, indicated by a net increase in intensity in the region $\delta_{iso} = -83$ to -94 ppm and a net decrease in intensity in the range $\delta_{iso} = -94$ to -115 ppm. This is most likely due to continued formation and polymerisation of the amorphous sodium silicate phase, as the Ca content is likely to have been depleted during the early stages of reaction.

3.2.4. Glass wool-based binder discussion

The main reaction product formed upon alkali activation of glass wool with both NaOH and $Na_2O{\cdot}2SiO_2$ is an X-ray amorphous sodium silicate gel as shown by SEM-EDX, XRD and NMR data. The gel chemistry is initially rich in Si and evolves as the reaction proceeds to incorporate more Na. A partially Ca-substituted N-(A-)S–H gel (denoted N-(C-)(A-)S–H) forms as an additional reaction product. is present with mainly Q^1, Q^2, and Q^2(1Al) Si units which continue to polymerise into longer chains with more Q^2 and Q^3 species as detected by ^{29}Si MAS NMR. However, as the content of Ca and Al are low in the precursor, at 8.2 wt% and 1.5 wt%, respectively, the content of this gel must be low.

The dissolution of precursor particles in NaOH-activated glass wool is extensive by 7 days, the microstructure of the gel formed densifies visibly and consequently the macroporosity of the binder decreases as shown by BSE-image analysis (Supporting information). The microstructure of the gel formed in $Na_2O{\cdot}2SiO_2$-activated glass wool is denser than that of NaOH-activated glass wool after curing for 1 day, and little difference is observed in the binder microstructure, morphology or macroporosity as the reaction progresses. Dissolution of glass wool in both NaOH and $Na_2O{\cdot}2SiO_2$ activators is incongruent, with preferential dissolution of Ca and Al at early stages of reaction according to the dissolution rate estimation method based on BSE-image analysis, XRF and EDX data reported in Supporting information. This is consistent with earlier results; sodium silicate solution can bind Ca and Al, thus removing them from the aqueous phase and accelerating their further dissolution from the precursor [57]. It is also possible that the gel formed in alkali-activated glass wools consists at least partly of hydrous alkali layered silicates and alkali silicate hydrates as the chemical composition of glass wool and alkali activator favour the formation of these types of gels [58–60], which contain primarily Q^3 Si sites, with smaller amounts of Q^1, Q^2 and Q^4 sites (consistent with the NMR data presented above).

Recently, soda-lime silicate glass with compositions similar to glass wool has been used as an AAM precursor [13,14,61]. The binder gel formed exhibited high strength in ambient dry conditions, but lacked hydrolytic stability in moist conditions (cured in a fog spray chamber). In order to improve the binder properties, some studies [13–17] mixed soda-lime silicate glass with metakaolin, slag or fly ash to provide extra Al and Ca to the reaction mixture creating water-insoluble gels [13,62,63]. Due to similar chemical compositions of soda-lime silicate glass and glass wool studied here, also the properties of glass wool-based binder could improve by using co-binders containing Al and Ca.

4. Conclusions

The phase assemblage and nanostructure of a series of alkali-activated mineral wools displaying varied chemical composition and mineralogy is resolved by application of advanced spectroscopic and microstructural characterisation techniques including X-ray diffraction, electron microscopy and solid state nuclear magnetic resonance spectroscopy.

Alkali activation of stone wool and glass wool with NaOH and $Na_2O{\cdot}2SiO_2$ solutions results in distinct reaction products due to the differences in reaction mixture chemical composition. The main reaction product formed in alkali-activated stone wool is an X-ray amorphous C-(N-)A-S-H-type gel, which is broadly comparable to those identified in alkali-activated GGBFS binders but displays greater disorder and lower Ca content. In the absence of a source of soluble Si (i.e. using NaOH as the activator) the gel chemical composition is initially Ca- and Al-rich, and evolves during the curing period to incorporate more Si as the reaction progresses. In the presence of a source of soluble Si (i.e. using $Na_2O{\cdot}2SiO_2$ as the activator) the gel chemical composition is initially rich in Si, and evolves during the curing period to incorporate more Ca and Al as the reaction progresses.

The presence of soluble Si in the reaction mixture also promotes increased aluminosilicate chain crosslinking in the C-(N-)A-S-H-type gel, as well as formation of an additional Al-rich N-A-S-H gel reaction product. The presence of significant amounts of MgO in stone wool results in formation of the Mg-rich LDH phase quintinite as an additional reaction product in NaOH-activated stone wool, however this is not observed when $Na_2O{\cdot}2SiO_2$ is used as the activator. Zeolite F (edingtonite-type) is also formed as an additional reaction product in NaOH-activated stone wool.

The main reaction product formed in alkali-activated glass wool is an X-ray amorphous sodium silicate gel (broadly comparable to soda-lime silicate glass) that is initially rich in Si and evolves as the reaction proceeds to incorporate more Na. Regardless of the activator used, a partially Ca- and Al-substituted sodium silicate glass (denoted N-(C-)(A-)S–H) forms as an additional reaction product. This glass comprises mainly Q^1, Q^2, and Q^2(1Al) Si units which continue to polymerise into longer chains with containing more Q^2 and Q^3 species.

Density of the binder microstructure of both alkali-activated stone and glass wool is promoted by the presence of soluble Si in the reaction mixture. In all alkali-activated mineral wool samples, mineral wool dissolution and partially dissolved fibre particles remain embedded in the binder matrix after curing for 7 days.

This work provides the most advanced description of the chemistry and structure of alkali-activated mineral wools to date, and reveals new insight that is crucial for controlling the mechanical properties, physical and chemical durability of these materials. This provides a new platform of knowledge to drive valorisation of mineral wool wastes and increased

sustainability in the construction industry.

Declaration of competing interest

The authors declare that they have no known competing financial interests or personal relationships that could have appeared to influence the work reported in this paper.

Acknowledgements

The research was performed under the auspices of Geodesign-project funded by the Business Finland (grant ID 1215/31/2015) and various companies (Boliden Harjavalta Oy, Destamatic Oy, Fortum Power and Heat Oy, Paroc Group Oy, Saint-Gobain Finland Oy, and Suomen Erityisjäte Oy). The experimental work was performed at the University of Sheffield, UK and at the University of Oulu, Finland. Dan Geddes, Dr Oday Hussein, Jarno Karvonen and Elisa Wirkkala are acknowledged for their assistance with some of the laboratory work. Dr Dale Prentice is acknowledged for assistance with SEM-EDX data processing and Dr Sandra van Meurs is acknowledged for her assistance acquiring NMR data. The authors thank the PQ Corporation for generously supplying the sodium silicate solution used in this investigation.

Appendix A. Supplementary data

Supplementary data to this article can be found online at https://doi.org/10.1016/j.cemconcomp.2019.103472.

References

[1] P.H.R. Borges, N. Banthia, H.A. Alcamand, W.L. Vasconcelos, E.H.M. Nunes, Performance of blended metakaolin/blastfurnace slag alkali-activated mortars, Cement Concr. Compos. 71 (2016) 42–52, https://doi.org/10.1016/j.cemconcomp.2016.04.008.

[2] G.V.P.B. Singh, K.V.L. Subramaniam, Influence of processing temperature on the reaction product and strength gain in alkali-activated fly ash, Cement Concr. Compos. 95 (2019) 10–18, https://doi.org/10.1016/j.cemconcomp.2018.10.010.

[3] B.C. McLellan, R.P. Williams, J. Lay, A. van Riessen, G.D. Corder, Costs and carbon emissions for geopolymer pastes in comparison to ordinary portland cement, J. Clean. Prod. 19 (2011) 1080–1090.

[4] A. Müller, B. Leydolph, K. Stanelle, Recycling mineral wool waste—technologies for the conversion of the fiber structure Part 1, Interceram 2009 (2009) 378–381.

[5] A.M. Papadopoulos, State of the art in thermal insulation materials and aims for future developments, Energy Build. 37 (2005) 77–86, https://doi.org/10.1016/j.enbuild.2004.05.006.

[6] EPA 11, 18 mineral wool manufacturing, in: Compil. Air Pollut. Emiss. Factors Vol. 1 Station. Point Area Sources, Office of Air Quality Planning and Standards, 1995. http://www3.epa.gov/ttn/chief/ap42/toc_kwrd.pdf.

[7] T.-A. Chen, J.-H. Chen, J.-S. Huang, Effects of activator and aging process on the compressive strengths of alkali-activated glass inorganic binders, Cement Concr. Compos. 76 (2017) 1–12, https://doi.org/10.1016/j.cemconcomp.2016.11.011.

[8] J. Yliniemi, O. Laitinen, P. Kinnunen, M. Illikainen, Pulverization of fibrous mineral wool waste, J. Mater. Cycles Waste Manag. 20 (2018) 1248–1256, https://doi.org/10.1007/s10163-017-0692-3.

[9] O. Väntsi, T. Kärki, Mineral wool waste in Europe: a review of mineral wool waste quantity, quality, and current recycling methods, J. Mater. Cycles Waste Manag. (2013) 1–11, https://doi.org/10.1007/s10163-013-0170-5 (2013).

[10] P. Kinnunen, J. Yliniemi, B. Talling, M. Illikainen, Rockwool waste in fly ash geopolymer composites, J. Mater. Cycles Waste Manag. 19 (2017) 1220–1227, https://doi.org/10.1007/s10163-016-0514-z.

[11] J. Yliniemi, P. Kinnunen, P. Karinkanta, M. Illikainen, Utilization of mineral wools as alkali-activated material precursor, Mater. Basel Switz. 9 (2016), https://doi.org/10.3390/ma9050312.

[12] J.L. Provis, J.S.J. van Deventer, Alkali Activated Materials - State-Of-The-Art Report, RILEM TC 224-AAM, 2014. https://www.rilem.net/docs/2014090109_star-224-aam_final-draft_full.pdf.

[13] R. Redden, N. Neithalath, Microstructure, strength, and moisture stability of alkali activated glass powder-based binders, Cement Concr. Compos. 45 (2014) 46–56, https://doi.org/10.1016/j.cemconcomp.2013.09.011.

[14] A.B. Pascual, M.T. Tognonvi, A. Tagnit-Hamou, Waste glass powder-based alkali-activated mortar, Nternational J. Res. Eng. Technol. 3 (2014) 15–19.

[15] C. Bobirică, J.-H. Shim, J.-Y. Park, Leaching behavior of fly ash-waste glass and fly ash-slag-waste glass-based geopolymers, Ceram. Int. 44 (2018) 5886–5893, https://doi.org/10.1016/j.ceramint.2017.12.085.

[16] T.H.A. Al Saadi, A.I. Badanoiu, A.I. Nicoara, S. Stoleriu, G. Voicu, Synthesis and properties of alkali activated borosilicate inorganic polymers based on waste glass, Constr. Build. Mater. 136 (2017) 298–306, https://doi.org/10.1016/j.conbuildmat.2017.01.026.

[17] S. Zhang, A. Keulen, K. Arbi, G. Ye, Waste glass as partial mineral precursor in alkali-activated slag/fly ash system, Cement Concr. Res. 102 (2017) 29–40, https://doi.org/10.1016/j.cemconres.2017.08.012.

[18] F. Puertas, M. Torres-Carrasco, Use of glass waste as an activator in the preparation of alkali-activated slag. Mechanical strength and paste characterisation, Cement Concr. Res. 57 (2014) 95–104, https://doi.org/10.1016/j.cemconres.2013.12.005.

[19] D.M. Bernstein, C. Morscheidt, A. De Meringo, M. Schumm, H.G. Grimm, U. Teichert, P. Thevenaz, L. Mellon, The biopersistence of fibres following inhalation and intratracheal instillation exposure, Ann. Occup. Hyg. 41 (1997) 224–230.

[20] T. Hirvijoki, Utilization of Mineral Wool Waste as Alkali-Activated Material Precursor, Master thesis, University of Oulu, 2018.

[21] A. Campopiano, A. Cannizzaro, F. Angelosanto, M.L. Astolfi, D. Ramires, A. Olori, S. Canepari, S. Iavicoli, Dissolution of glass wool, rock wool and alkaline earth silicate wool: morphological and chemical changes in fibers, Regul. Toxicol. Pharmacol. 70 (2014) 393–406, https://doi.org/10.1016/j.yrtph.2014.05.023.

[22] A. Cheng, W.-T. Lin, R. Huang, Application of rock wool waste in cement-based composites, Mater. Des. 32 (2011) 636–642, https://doi.org/10.1016/j.matdes.2010.08.014.

[23] V. Sal'nikov, Properties of mineral wool after long operation in walls of buildings in Middle Ural region, Build Mater Stroit. Mater. 3 (2003) 42–43.

[24] E. Nielsen, P. Nørhede, O. Ladefoged, L. Tobiassen, Evaluation of Health Hazards by Exposure to Mineral Wools (Glass, Stone/slag, HT) and Proposal of a Health-Based Quality Criterion for Ambient Air, 2013. Copenhagen, Denmark, https://www2.mst.dk/Udgiv/publications/2013/12/978-87-93026-68-1.pdf.

[25] C.A. Rees, J.L. Provis, G.C. Lukey, J.S.J. van Deventer, The mechanism of geopolymer gel formation investigated through seeded nucleation, Colloids Surf. Physicochem. Eng. Asp. 318 (2008) 97–105, https://doi.org/10.1016/j.colsurfa.2007.12.019.

[26] A. Fernández-Jiménez, A. Palomo, M. Criado, Microstructure development of alkali-activated fly ash cement: a descriptive model, Cement Concr. Res. 35 (2005) 1204–1209, https://doi.org/10.1016/j.cemconres.2004.08.021.

[27] R.R. Lloyd, J.L. Provis, J.S.J. van Deventer, Microscopy and microanalysis of inorganic polymer cements. 1: remnant fly ash particles, J. Mater. Sci. 44 (2009) 608–619, https://doi.org/10.1007/s10853-008-3077-0.

[28] R.R. Lloyd, J.L. Provis, J.S.J. van Deventer, Microscopy and microanalysis of inorganic polymer cements. 2: the gel binder, J. Mater. Sci. 44 (2009) 620–631, https://doi.org/10.1007/s10853-008-3078-z.

[29] R.P. Williams, R.D. Hart, A. van Riessen, Quantification of the extent of reaction of metakaolin-based geopolymers using X-ray diffraction, scanning electron microscopy, and energy-dispersive spectroscopy, J. Am. Ceram. Soc. 94 (2011) 2663–2670, https://doi.org/10.1111/j.1551-2916.2011.04410.x.

[30] I. Ismail, S.A. Bernal, J.L. Provis, R. San Nicolas, S. Hamdan, J.S.J. van Deventer, Modification of phase evolution in alkali-activated blast furnace slag by the incorporation of fly ash, Cement Concr. Compos. 45 (2014) 125–135, https://doi.org/10.1016/j.cemconcomp.2013.09.006.

[31] J.S.J. van Deventer, R.S. Nicolas, I. Ismail, S.A. Bernal, D.G. Brice, J.L. Provis, Microstructure and durability of alkali-activated materials as key parameters for standardization, J. Sustain. Cem.-Based Mater. 4 (2015) 116–128, https://doi.org/10.1080/21650373.2014.979265.

[32] A. Fernández-Jiménez, A. Palomo, Composition and microstructure of alkali activated fly ash binder: effect of the activator, Cement Concr. Res. 35 (2005) 1984–1992, https://doi.org/10.1016/j.cemconres.2005.03.003.

[33] F. Winnefeld, A. Leemann, M. Lucuk, P. Svoboda, M. Neuroth, Assessment of phase formation in alkali activated low and high calcium fly ashes in building materials, Constr. Build. Mater. 24 (2010) 1086–1093.

[34] B. Walkley, R. San Nicolas, M.-A. Sani, J.D. Gehman, J.S.J. van Deventer, J. L. Provis, Phase evolution of Na_2O–Al_2O_3–SiO_2–H_2O gels in synthetic aluminosilicate binders, Dalton Trans. 45 (2016) 5521–5535, https://doi.org/10.1039/C5DT04878H.

[35] S.A. Bernal, R. San Nicolas, R.J. Myers, R. Mejía de Gutiérrez, F. Puertas, J.S.J. van Deventer, J.L. Provis, MgO content of slag controls phase evolution and structural changes induced by accelerated carbonation in alkali-activated binders, Cem, Concr. Res. 57 (2014) 33–43, https://doi.org/10.1016/j.cemconres.2013.12.003.

[36] M. Ben Haha, B. Lothenbach, G. Le Saout, F. Winnefeld, Influence of slag chemistry on the hydration of alkali-activated blast-furnace slag — Part I: effect of MgO, Cement Concr. Res. 41 (2011) 955–963, https://doi.org/10.1016/j.cemconres.2011.05.002.

[37] S.A. Bernal, J.L. Provis, B. Walkley, R. San Nicolas, J.D. Gehman, D.G. Brice, A. R. Kilcullen, P. Duxson, J.S.J. van Deventer, Gel nanostructure in alkali-activated binders based on slag and fly ash, and effects of accelerated carbonation, Cement Concr. Res. 53 (2013) 127–144, https://doi.org/10.1016/j.cemconres.2013.06.007.

[38] J.L. Provis, G.C. Lukey, J.S.J. van Deventer, Do geopolymers actually contain nanocrystalline zeolites? A reexamination of existing results, Chem. Mater. 17 (2005) 3075–3085, https://doi.org/10.1021/cm050230i.

[39] R. Gellert, Inorganic mineral materials for insulation in buildings. 8.5.1 Mineral wool, in: Mater. Energy Effic. Therm. Comf. Build, Woodhead Publishing in Energy, UK, 2010, pp. 193–228.

[40] S.-D. Wang, K.L. Scrivener, 29 Si and 27 Al NMR study of alkali-activated slag, Cement Concr. Res. 33 (2003) 769–774, https://doi.org/10.1016/S0008-8846(02)01044-X.

[41] I.G. Richardson, The calcium silicate hydrates, Cement Concr. Res. 38 (2008) 137–158, https://doi.org/10.1016/j.cemconres.2007.11.005.

[42] R.J. Myers, S.A. Bernal, R. San Nicolas, J.L. Provis, Generalized structural description of calcium–sodium aluminosilicate hydrate gels: the cross-linked substituted tobermorite model, Langmuir 29 (2013) 5294–5306, https://doi.org/10.1021/la4000473.

[43] B. Walkley, R. San Nicolas, M.-A. Sani, G.J. Rees, J.V. Hanna, J.S.J. van Deventer, J.L. Provis, Phase evolution of C-(N)-A-S-H/N-A-S-H gel blends investigated via alkali-activation of synthetic calcium aluminosilicate precursors, Cement Concr. Res. 89 (2016) 120–135, https://doi.org/10.1016/j.cemconres.2016.08.010.

[44] P. Duxson, J.L. Provis, G.C. Lukey, F. Separovic, J.S.J. van Deventer, ^{29}Si NMR Study of structural ordering in aluminosilicate geopolymer gels, Langmuir 21 (2005) 3028–3036, https://doi.org/10.1021/la047336x.

[45] S.J. Mills, A.G. Christy, J.-M.R. Génin, T. Kameda, F. Colombo, Nomenclature of the hydrotalcite supergroup: natural layered double hydroxides, Mineral. Mag. 76 (2012) 1289–1336, https://doi.org/10.1180/minmag.2012.076.5.10.

[46] X. Ke, S.A. Bernal, J.L. Provis, Controlling the reaction kinetics of sodium carbonate-activated slag cements using calcined layered double hydroxides, Cement Concr. Res. 81 (2016) 24–37, https://doi.org/10.1016/j.cemconres.2015.11.012.

[47] iza-onlineorg, Edingtonite, IZA-Onlineorg, 2018. http://www.iza-online.org/natural/Datasheets/Edingtonite/edingtonite.htm.

[48] P.T. Durdziński, M. Ben Haha, M. Zajac, K.L. Scrivener, Phase assemblage of composite cements, Cement Concr. Res. 99 (2017) 172–182, https://doi.org/10.1016/j.cemconres.2017.05.009.

[49] I.G. Richardson, G.W. Groves, Microstructure and microanalysis of hardened cement pastes involving ground granulated blast-furnace slag, J. Mater. Sci. 27 (1992) 6204–6212, https://doi.org/10.1007/BF01133772.

[50] R. Taylor, I.G. Richardson, R.M.D. Brydson, Composition and microstructure of 20-year-old ordinary Portland cement–ground granulated blast-furnace slag blends containing 0 to 100% slag, Cement Concr. Res. 40 (2010) 971–983, https://doi.org/10.1016/j.cemconres.2010.02.012.

[51] X. Cong, R.J. Kirkpatrick, Hydration of calcium aluminate cements: a Solid-State ^{27}Al NMR Study, J. Am. Ceram. Soc. 76 (1993) 409–416, https://doi.org/10.1111/j.1151-2916.1993.tb03799.x.

[52] C.S. Walker, S. Sutou, C. Oda, M. Mihara, A. Honda, Calcium silicate hydrate (C-S-H) gel solubility data and a discrete solid phase model at 25 °C based on two binary non-ideal solid solutions, Cement Concr. Res. 79 (2016) 1–30, https://doi.org/10.1016/j.cemconres.2015.07.006.

[53] A. Kumar, B.J. Walder, A. Kunhi Mohamed, A. Hofstetter, B. Srinivasan, A. J. Rossini, K. Scrivener, L. Emsley, P. Bowen, The atomic-level structure of cementitious calcium silicate hydrate, J. Phys. Chem. C 121 (2017) 17188–17196, https://doi.org/10.1021/acs.jpcc.7b02439.

[54] R.J. Myers, S.A. Bernal, J.D. Gehman, J.S.J. van Deventer, J.L. Provis, The role of Al in cross-linking of alkali-activated slag cements, J. Am. Ceram. Soc. 98 (2015) 996–1004, https://doi.org/10.1111/jace.13360.

[55] I. Garcia-Lodeiro, A. Palomo, A. Fernández-Jiménez, D.E. Macphee, Compatibility studies between N-A-S-H and C-A-S-H gels. Study in the ternary diagram Na_2O–CaO–Al_2O_3–SiO_2–H_2O, Cement Concr. Res. 41 (2011) 923–931, https://doi.org/10.1016/j.cemconres.2011.05.006.

[56] X.X. Xue, J.F. Stebbins, M. Kanzaki, P.F. McMillan, B. Poe, Pressure-induced silicon coordination and tetrahedral structural changes in alkali oxide-silica melts up to 12 GPa: NMR, Raman, and infrared spectroscopy, Am. Mineral. (1991) 8–26.

[57] S.A. Bernal, J.L. Provis, A. Fernández-Jiménez, P. Krivenko, E. Kavalerova, M. Palacios, C. Shi, Binder chemistry - high-calcium alkali-activated materials, in: Alkali Activated Materials - State-Of-The-Art Rep., Springer Netherlands, 2014, pp. 59–91. https://www.rilem.net/docs/2014090109_star-224-aam_final-draft_full.pdf.

[58] R.J. Kirkpatrick, Experimental and molecular dynamics modeling studies of interlayer swelling: water incorporation in kanemite and ASR gel, Mater. Struct. 38 (2005) 449–458, https://doi.org/10.1617/14344.

[59] D.C. Apperley, M.J. Hudson, M. Keene, J. Knowles, Kanemite ($NaHSi_2O_5$*$3H_2O$) and its hydrogen-exchanged form, J. Mater. Chem. 5 (1995) 577–582.

[60] A.R. Brough, C.M. Dobson, I.G. Richardson, G.W. Growes, Alkali activation of reactive silicas in cements: in situ ^{29}Si MAS NMR studies of the kinetics of silicate polymerization, J. Mater. Sci. 31 (1996) 3365–3373.

[61] M. Torres-Carrasco, C. Rodríguez-Puertas, M. del M. Alonso, F. Puertas, Alkali activated slag cements using waste glass as alternative activators. Rheological behaviour, Bol. Soc. Esp. Cerámica Vidr. 54 (2015) 45–57, https://doi.org/10.1016/j.bsecv.2015.03.004.

[62] I. Giannopoulou, D. Panias, Hydrolytic stability of sodium silicate gels in the presence of aluminum, J. Mater. Sci. 45 (2010) 5370–5377, https://doi.org/10.1007/s10853-010-4586-1.

[63] P.W. Brown, The system Na_2O-CaO-SiO_2-H_2O, J. Am. Ceram. Soc. 73 (1990) 5.